Chemical Science

ROYAL SOCIETY OF CHEMISTRY

EDGE ARTICLE

View Article Online
View Journal | View Issue

Cite this: *Chem. Sci.*, 2024, **15**, 7150

All publication charges for this article have been paid for by the Royal Society of Chemistry

Received 30th January 2024
Accepted 25th March 2024

DOI: 10.1039/d4sc00723a

rsc.li/chemical-science

Visible-light TiO_2-catalyzed synthesis of dihydrobenzofurans by oxidative [3 + 2] annulation of phenols with alkenyl phenols†

Jingze Wu, Yaning Liu and Marisa C. Kozlowski *

An oxidative strategy for the preparation of dihydrobenzofurans *via* heterogeneous photocatalysis is reported. This method leverages the surface interaction between the alkenyl phenol and the TiO_2 solid surface, which enables direct activation by visible light without the need for pre-functionalization or surface modification. The resulting alkenyl phenoxyl radical is proposed to be selectively captured by a neutral phenol nucleophile, rendering β-5′ coupling with excellent chemo- and regio-selectivity. The reaction proceeds under benign conditions, using an inexpensive, nontoxic, and recyclable photocatalyst under visible light irradiation with air as the terminal oxidant at room temperature.

Introduction

Phenols and their derivatives function as essential building blocks for various classes of complex molecules, playing crucial roles in biological systems.[1] Lignans, for example, are phenol-derived natural products abundant in nature that exhibit unique structural patterns and versatile biological functions, sparking considerable attention toward their controlled synthesis. Within this class, neo-lignans derived from alkenyl phenols comprise a range of natural products (Fig. 1).[2] Such structures arise from oxidation of alkenyl phenols by peroxidases or laccases to the radical intermediates that are stabilized through resonance (Scheme 1).[3] Subsequently, radical couplings among these resonance forms have the potential to generate a diverse array of distinct structures *via* selective dimerization. In recent years, radical-based reactions have gained prominence as powerful tools for bond formation. And in this context, the reaction between alkenyl phenoxyl radicals and neutral alkenyl phenol nucleophiles offers intriguing opportunities for the construction of lignan homodimers. In 2019, the Kozlowski group reported a vanadium catalyzed homo-coupling of alkenyl phenols to selectively generate β–β and β-O homodimers.[4]

Within the realm of lignan scaffolds, the heterodimers possessing a dihydrobenzofuran core through β-5′ coupling stand out as subjects of significant interest due to a diverse spectrum of bioactivities, encompassing antioxidant, anti-inflammatory, antiparasitic, neuroprotective, and anticancer activities, among others.[5] As a highly reactive species, the alkenyl phenoxyl radical possesses the potential to engage in selective C–C bond formation with neutral phenol partners. Achieving such selectivity, however, remains challenging due to the inherent complexity of radical reactions and the competing pathways of homo-coupling *versus* cross-coupling.[6]

Previous attempts for selective generation of β-5′ lignan heterodimers have been reported by means of enzymatic processes or bio-mimicking strategies.[7] Recently, cross-

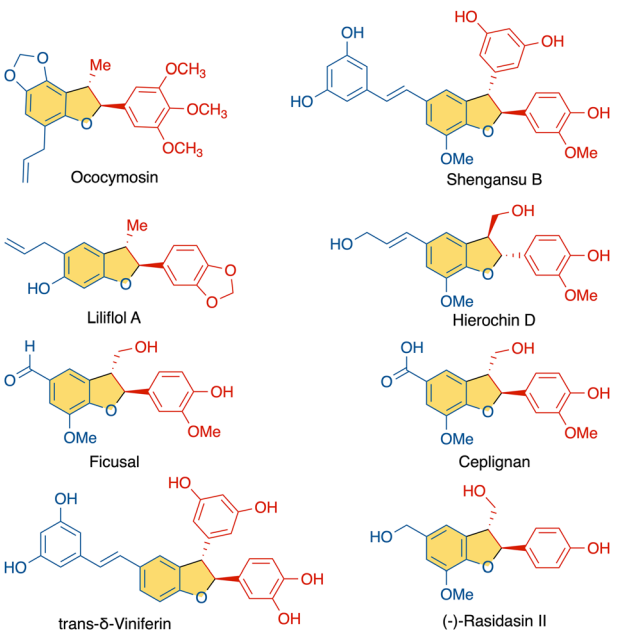

Fig. 1 Naturally occurring β-5′ neolignans (selected examples).

Department of Chemistry, Roy and Diana Vagelos Laboratories, University of Pennsylvania, Philadelphia, Pennsylvania 19104, USA. E-mail: marisa@sas.upenn.edu

† Electronic supplementary information (ESI) available: Experimental procedures and NMR spectral copies (PDF), FAIR data, including the primary NMR FID files for compounds (ZIP) and computational coordinates (*XYZ*). See DOI: https://doi.org/10.1039/d4sc00723a

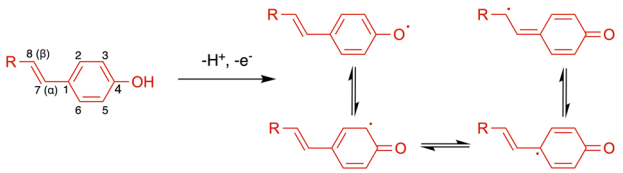

Scheme 1 Resonance forms of phenoxyl radical from by one-electron oxidation.

couplings of alkenyl anisoles and phenols for selective β-5′ coupling have been reported by several groups (Scheme 2a–c), however, these reported methods require use of O-protected alkenyl anisoles.[8–11] Furthermore, the accessibility of bespoke covalent organic framework (COF) catalysts poses a challenge for general use (Scheme 2c).

Selective cross-coupling of alkenyl phenols with other alkenyl phenols or with phenols is challenging due to several reactive sites as shown in Scheme 1 and the potential for homocoupling of either partner. As such there are limited reports of such coupling. One approach to this challenge has been the use of one far more oxidizable partner such as a *para*-aminophenol as reported by the Liu group using catalytic copper acetate

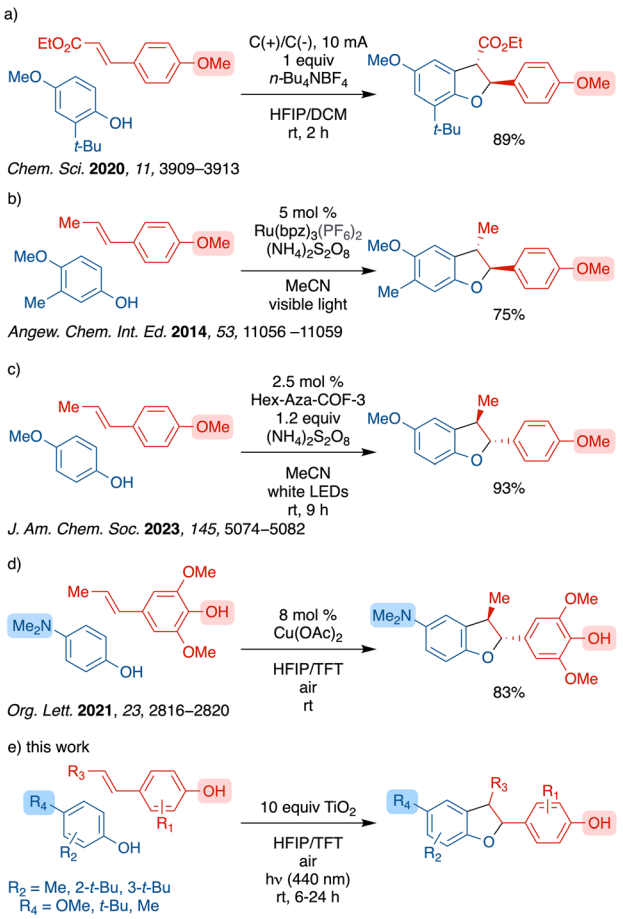

Scheme 2 Previous strategies for lignan dihydrobenzofuran synthesis, (a) electrochemical method, (b) photocatalytic method using a ruthenium photocatalyst, (c) photocatalytic method using a COF catalyst, (d) copper acetate method, (e) this work.

(Scheme 2d).[12] However, there has been no general selective cross-couplings of alkenyl phenols in less activated systems.

The application of titanium dioxide (TiO_2) as a photocatalyst is much less common in organic synthesis relative to metal-organic and organic photocatalysts. Most TiO_2 catalyzed reactions typically utilize UV light, employ an adsorbate as the sensitizer to improve visible light absorption, or apply surface doping to lower the band gap.[13] In contrast, there are limited examples where the substrate enables visible light absorption by forming an LMCT complex. Heteroatom-bearing substrates, such as amines,[14] sulfides,[15] diazoniums[16] and benzyl alcohols,[17] have been shown to form such LMCT complexes with unmodified TiO_2 to achieve oxidation. However, TiO_2–LMCT complexes with phenolic substrates remain underexplored.[18] In 2023, we reported an oxidative synthesis of diphenols through a heterogeneous titanium dioxide (TiO_2) photocatalyst where the phenol served a dual role as both the substrate and the photosensitizer.[19] Further, we discovered that the dihydrobenzofuran core of the iso-eugenol homodimer, licarin A, can be selectively formed using TiO_2 under blue light irradiation with excellent yield and stereoselectivity.[19] We hypothesized that an interaction of the hydroxy group of the alkenyl phenol with TiO_2 would enable selective generation of the lignan dihydrobenzofuran cores through cross-coupling between alkenyl phenols and phenols with a broader functional group tolerance. Herein, we report the first TiO_2 photocatalyzed selective oxidative β-5′ cross-coupling of alkenyl phenols and phenols for the generation of lignan dihydrobenzofuran cores.

Results and discussion

Exploration of the cross-coupling reaction between phenols and alkenyl phenols began with the readily oxidized substrate and easily available iso-eugenol (**2a**) with 2-*tert*-butyl-4-methoxyphenol (**1a**) (see in ESI† for full optimization table). An excess of TiO_2 powder (10.0 equiv.) was used considering the limited surface area as reactions will only occur on the TiO_2 solid surface (0.1 equiv. of TiO_2 gave <10% conversion after 12 h). The exceptionally low cost and facile recyclability of TiO_2 by centrifugation offsets this high loading. Hexafluoroisopropanol (HFIP) was used as it generally facilitates phenolic couplings.[20–26] Initial reaction began with an excess of **2a** (3.0 equiv.), however, only 2% of cross coupled **3aa** was isolated, and 79% of **2a** underwent homocoupling to generate licarin A, and 83% of the unreacted **1a** was recovered (entry 1). Reducing the equivalence of **2a** from 3.0 to 1.5 improved the yield of heterodimer **3aa** significantly, from 2% to 32%, and 63% of the unreacted **1a** was recovered (entry 2). Doubling the reaction time from 6 to 12 h only slightly increased the yield, from 32% to 38% (entry 3). Further reduction from 1.5 to 1.0 equivalents of **2a** improved the yield from 32% to 42% (entry 4). A significant improvement in yield of **3aa** (59%) was observed with an excess **1a** (2.0 equiv.) (entry 5). Use of an HFIP/MeCN mixture offered no advantage (entry 6) but use of HFIP with trifluorotoluene (TFT) did improve the yield (entry 7) with the balance of limiting reagent **2a** forming homodimer. Finally, use

Table 1 Reaction condition optimization[a]

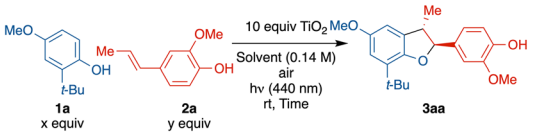

Entry	Solvent	**1a** (*x* equiv.)	**2a** (*y* equiv.)	Time (h)	**2a** homodimer[b] (%)	Yield **3aa**[b] (%)
1	HFIP	1.0	3.0	6	81	2
2	HFIP	1.0	1.5	6	50	32
3	HFIP	1.0	1.5	12	53	38
4	HFIP	1.0	1.0	6	46	42
5	HFIP	2.0	1.0	6	24	59
6	HFIP/MeCN (1 : 1)	2.0	1.0	6	19	51
7	**HFIP/TFT (1 : 1)**	**2.0**	**1.0**	**6**	**21**	**66**
8	HFIP/TFT (1 : 1)	5.0	1.0	6	14	37

[a] Reaction conditions: **1a** (0.56 mmol), 4.0 mL solvent, 6–12 h. [b] Isolated yield.

of an even greater excess of **1a** (5.0 equiv.) was not effective (entry 8). Longer reaction times with optimal conditions (entry 7) resulted in overoxidation products (see Fig. S25 and S26†). Examination of a homogenous photocatalyst ($MesAcr^{+}BF4^{-}$), in analogy to the work of Yoon and coworkers,[9] resulted in 14% yield with poor chemo-selectivity and poor mass balance (see ESI† for details).

Control experiments without light (Table 2, entry 1), air/oxygen (entry 2), or TiO_2 (entry 3) all failed to provide any product, showing all three components are necessary.

With the optimized conditions established, we then proceeded to evaluate the scope of this protocol (Scheme 3). Gram-scale synthesis using the same light source provided **3aa** in a lower yield (39%), likely due to limited light penetration of the larger vessel. For the phenol component **1**, use of a smaller *ortho*-group (Me *vs.* *t*-Bu) led to **3ca** with a similar yield (57%) relative to **3aa** (66%). In comparison to prior work (Scheme 2d) which required very electron-rich phenols, this method was successful with electron-neutral phenols, albeit with lower yields (comparing **3db** 24% with **3ab** 71% and **3eb** 32% with **3cb** 60%). *meta*-Substitution of the phenol in **3bb** was also tolerated but resulted in lower yield (43%) compared to the *ortho*-congener **3ab** (71%). *N*-Acetyl indole derived phenols did not react whereas a carbazole derived phenol (**1f**) underwent rapid oxidation to multiple products, giving diminished yield of **3fb** in 27% with a poor diastereomeric ratio. In addition, more complex phenols such as piperazine derived phenol, aryl substituted phenol and dibenzofuran derived phenol all showed reactivity toward cross coupling with an alkenyl phenol, giving **3eg** (65%), **3ig** (88%) and **3hg** (38%).

For the aryl ring of alkenyl phenol component **2**, additional methoxy substitution in **3ab** (71%) and **3cb** (60%) led to slightly improved yields relative to **3aa** (66%) and **3ca** (57%). Replacing the phenol of this portion entirely with a dimethylamino arene results in good yield of **3af** (61%) relative to the methoxyphenol **3aa** (66%) or the dimethoxyphenol **3ab** (71%). For alkenyl phenol component **2**, substitution on the alkenyl terminus exerted a profound influence on the reaction outcomes. Specifically, a lack of substitution as in **3ad** and **3ac** resulted in significantly diminished yields (37% and 17%). On the other hand, alkenes with a dimethoxyphenyl or a nitrophenyl substituent led to pronounced improvements, most likely due to greater stabilization of the intermediate radial, forming **3ae** and **3ig** in 79% and 88% yield, respectively. Notably, this method is complementary to that using $Cu(OAc)_2$ (ref. 12) from Scheme 2d which gave no reactivity with the substrates for **3ig** (see ESI† for details). Changing the electronic characteristics of the alkenyl phenyl substituent at the β-position from electron rich to electron poor such as **3ig**, **3ag**, **3eg** and **3ih** resulted in 88%, 69%, 65% and 41% yield. Other alkenyl phenols with alkyl substitution on the aromatic ring were not stable (decomposed upon storage at −20 °C) and gave complex mixtures with no cross-coupling observed (see ESI† for details).

Visible light activation of TiO_2 can be achieved by means of surface interaction with adsorbates that do not absorb visible

Table 2 Control reactions[a]

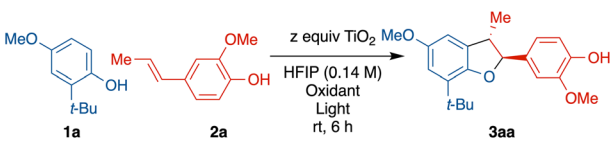

Entry	TiO_2 (*z* equiv.)	Light	Oxidant	Yield **3aa** (%)
1	10	Dark[b]	Air	—
2	10	440 nm	Argon	—
3	—	440 nm	Air	—

[a] Reaction conditions: **1a** (1.12 mmol), **2a** (0.56 mmol) 4.0 mL solvent, 12 h. [b] Reaction ran without light source; reaction flask wrapped with foil.

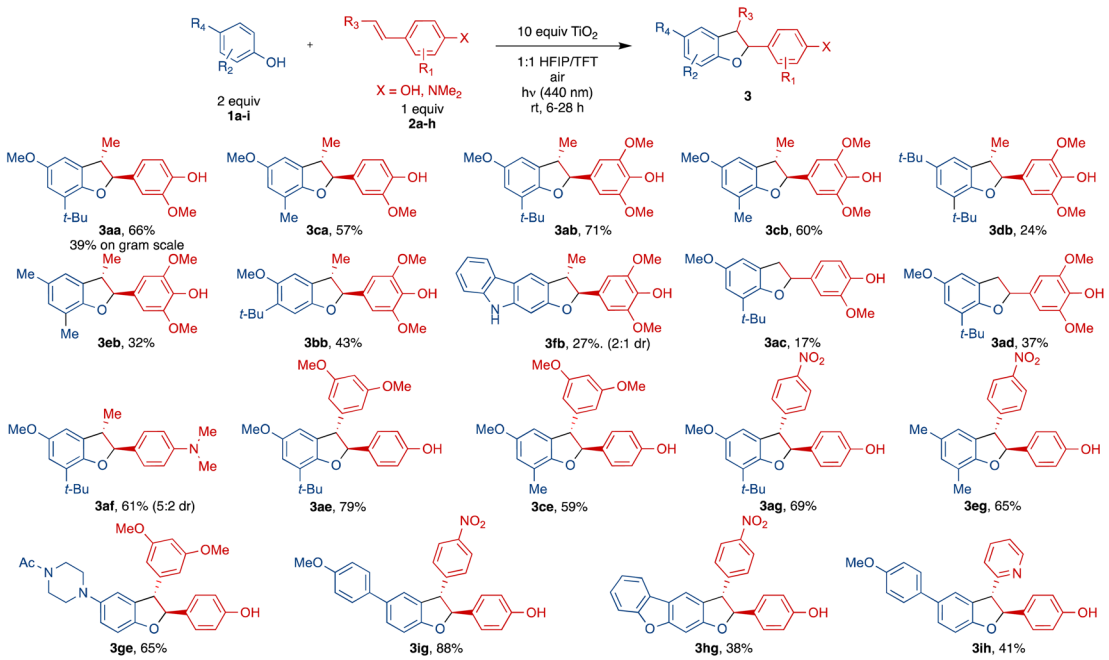

Scheme 3 Substrate scope. See ESI† for reaction conditions.

light themselves *via* ligand to metal charge transfer (LMCT) from the highest occupied molecular orbital (HOMO) of the adsorbates to the conduction band (CB) of TiO_2.[27] Next, the oxidized adsorbate may either undergo further reactions with an electron donor or regenerate the neutral adsorbate *via* back electron transfer (BET) (Fig. 2).[28] In this reaction, photocatalytic reactivity was observed under 440 nm light irradiation, while neither reaction component exhibits visible light absorption.[29] To explain this phenomenon, we hypothesized that the surface interaction between the TiO_2 semiconductor and phenols plays a crucial role in phenol activation and the subsequent reactivity.

Adding alkenyl phenol **2a** to white TiO_2 powder causes an immediate colour change indicating a red shift in the absorption and emission spectra (Fig. 3a). Fig. 3b shows the Raman spectra of **2a** and TiO_2–**2a**. The sharp and intense peak at 1265.7 cm^{-1} of **2a** was assigned to the alkenyl phenol C–O and/or C–O–H vibrations in accord with prior literature measurements.[30] Binding of **2a** to the solid surface leads to a significant drop in intensity of this signal, indicating substantive structural changes around the hydroxy group which results in changes in polarity. The new intense peak at 1276.98 cm^{-1} in TiO_2–**2a** was attributed to a Ti–O–C linkage.[31] To further characterize the structural changes upon surface attachment, FT-IR spectra comparing 4-methylphenol and the TiO_2-bound version were obtained (Fig. 3c). 4-Methylphenol was chosen instead of **2a** as it gave a clearer signal for the O–H vibrations. Frequency analyses were performed [UB3LYP-D3/6-31G(d,p) see ESI† for details] for visualization and vibrational assignments. 4-Methylphenol shows an intense peak around 1222 cm^{-1}, which was assigned to O–H bending vibrations. Upon surface binding, the broad peak around 1244 cm^{-1} was attributed to vibrations that resulted from a Ti–O–C linkage. The sharp peak around 1520 cm^{-1} for a methyl rotation did not undergo significant shifting upon surface binding. Similarly, the two adjacent peaks around 1600 cm^{-1} and 1630 cm^{-1} that were assigned to the symmetric and asymmetric stretching of the C=C bonds also remained unchanged. Combined, these findings indicate significant structural changes around the phenol hydroxy group, resulting from the formation of a Ti–O–C linkage, consistent with previous reports.[31]

Electronic excitation spectra and spatial electron distribution profiles were generated using TD-DFT [TD-UB3LYP-D3/6-31G(d,p)-SDD(Ti), see ESI† for details] with an anatase Ti tetramer cluster model complex.[32] The TiO_2 cluster was frozen during geometry optimization to maintain the anatase structure while all other atoms were allowed to relax. The simulated electronic excitation spectra in Fig. 3d shows two major excitations in the UVB and UVC region for unbound **2a**. There is a significant red shift of this signal upon formation of an adduct

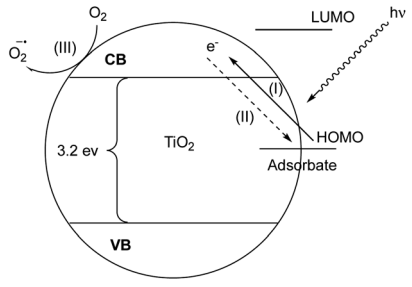

Fig. 2 TiO_2 visible-light LMCT sensitization: (I) visible-light induced LMCT transfer, (II) charge recombination, (III) electron transfer to a terminal oxidant, valence band (VB), conduction band (CB).

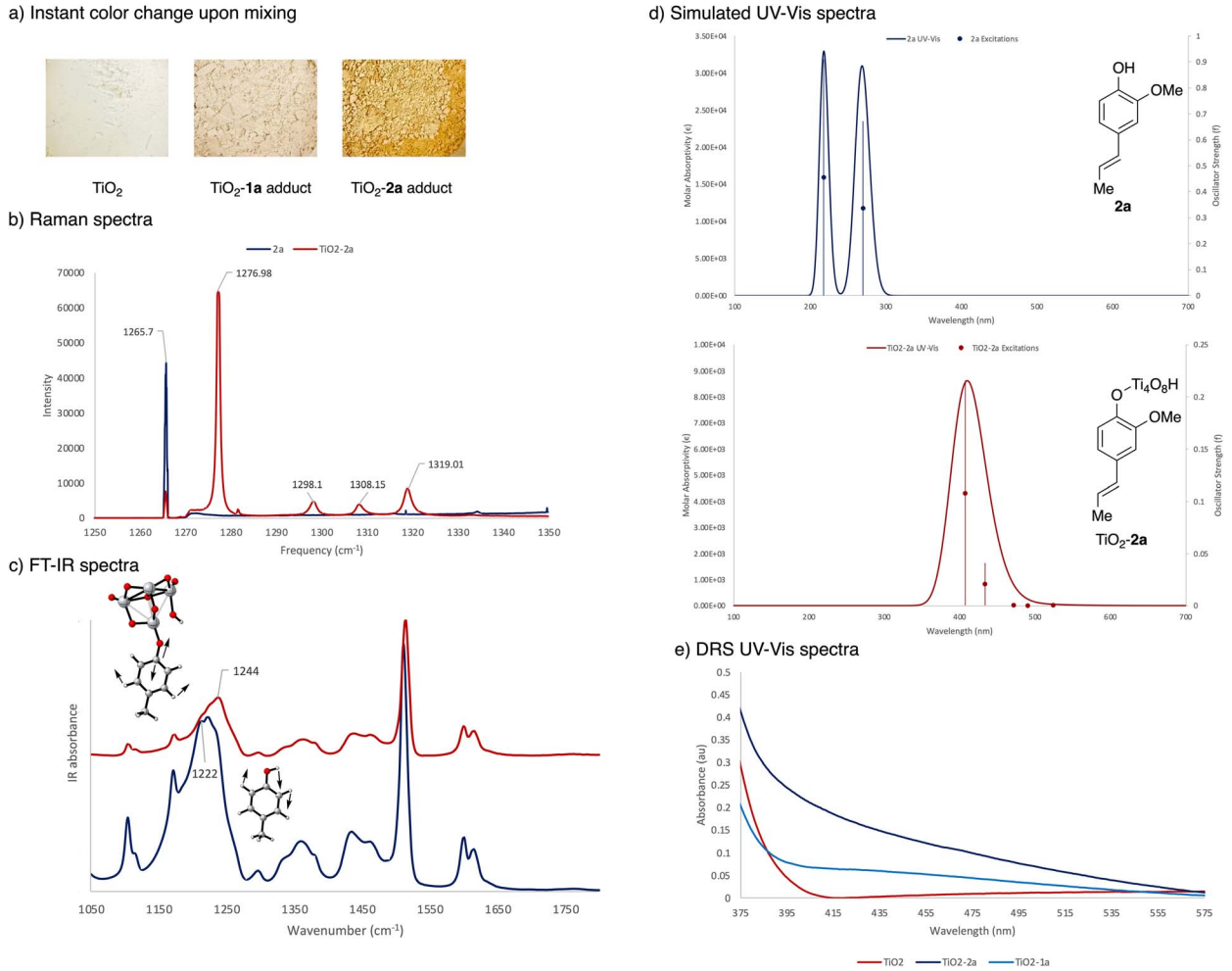

Fig. 3 (a) Color change upon addition of **2a** to TiO_2, (b) Raman spectra comparing **2a** and TiO_2-bound **2a**, (c) FT-IR spectra comparing 4-methylphenol and the TiO_2-bound version, vibrational modes assigned using UB3LYP-D3/6-31G(d,p), (d) simulated UV-Vis spectra of **2a** and TiO_2-bound **2a** generated using TD-UB3LYP-D3/6-31G(d,p)-SDD(Ti), (e) Kubelka–Munk transformations of diffuse reflection data of **2a** and TiO_2-bound **2a**.

with TiO_2, consistent with both the colour change observed in the reaction and with the experimental diffuse reflectance data (Fig. 3e). Notably, this new absorption band from 350–525 nm coincides with the wavelength of light (440 nm Kessil lamp) used in the photocatalysis. In comparing the surface association of **1a** *vs.* **2a**, TiO_2–**2a** showed a stronger absorption signal around 440 nm, consistent with the more intense color change observed, indicating that the TiO_2–**2a** adduct is being activated preferentially under reaction conditions.

Fig. 4a shows the calculated energy levels of **2a** and **1a**, alongside with the valence and conduction band of TiO_2.[33] Both the photocatalyst and the substrates were found to exhibit wide band gap (3.2 eV) and HOMO–LUMO gaps (4.6 eV and 5.3 eV) outside of the visible range, excluding the possibility for direct excitation of either component. Aligned with our hypothesis, the energy gap between **2a** HOMO and TiO_2 conduction band is significantly lowered (1.5 eV) upon surface attachment, within the wavelength of light (440 nm Kessil lamp) used in the reaction.

The spatial distribution of the highest, second, and third highest occupied molecular orbitals (HOMO, HOMO−1, HOMO−2), as well as the lowest, second, and third lowest unoccupied molecular orbitals (LUMO, LUMO+1, LUMO+2) in Fig. 4b, reveals the direction of the charge transfer. The electron density in HOMO, HOMO−1, and HOMO−2 is distributed throughout the alkenyl phenol π-conjugation. The LUMO, LUMO+1, and LUMO+2, which correspond to the conduction band of TiO_2, on the other hand, have electron density predominantly concentrate on the TiO_2 cluster moiety. Thus, it becomes clear that the photoinduced LMCT occurs across the interface joined by the alkenyl phenol HOMO and TiO_2 conduction band.[35] This surface attachment effectively bypasses the wide band gap of the semiconductor and allows for direct photoactivation by visible light, achieving similar effects as doping without the need for surface modification.

To gain further insights into the reaction mechanism and the observed selectivity, kinetics experiments and DFT calculations were undertaken (Fig. 5). In order to pinpoint which

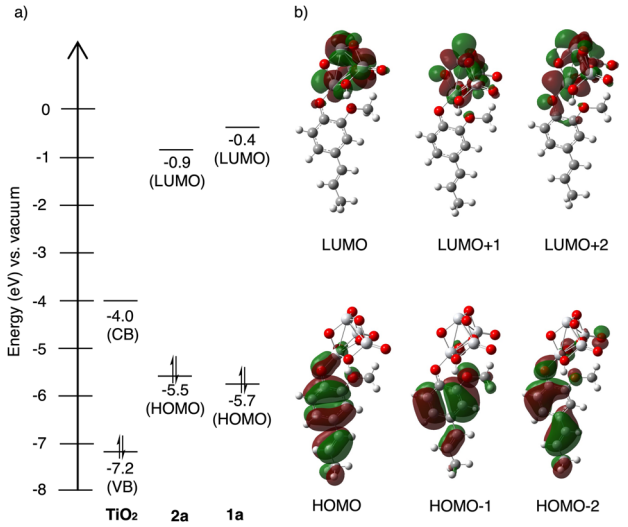

Fig. 4 (a) energy level diagram of **2a** and **1a** calculated using RB3LYP/6-311+(d,p), alongside with the valence and conduction band of TiO_2, (b) spatial electron distributions of HOMO, HOMO−1, HOMO−2, LUMO, LUMO+1, LUMO+2 of the TiO_2–**2a** adduct calculated using TD-UB3LYP-D3/6-31G(d,p)-SDD(Ti).

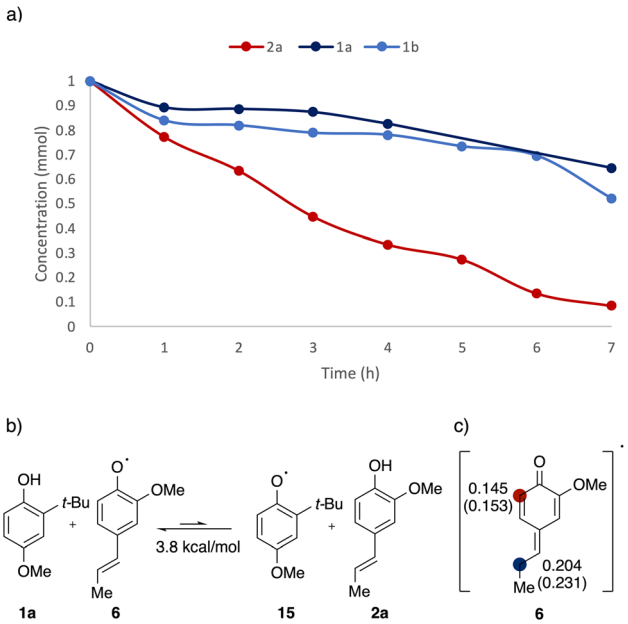

Fig. 5 (a) Kinetics of **2a** *vs.* **1a** *vs.* **1b**. Yield for **2a** determined *via* UPLC using 4-ethylanisole as the internal standard; yield for **1a** and **1b** determined *via* UPLC using 1,3,5-trimethoxybenzene as the internal standard, (b) thermodynamic stability of **6** *vs.* **15**. Free energies were computed using UM06/6-311++G(d,p)-CPCM(HFIP)//UB3LYP-D3/6-31G(d,p). (c) Spin density distribution of *ortho*- *vs.* β-sites calculated using population analysis. Numbers outside parentheses are derived from NBO spin, numbers inside are from Mulliken spin.

component is being activated predominately, decay of starting materials was monitored over the course of the reaction (Fig. 5a). After three hours, over half of **2a** was consumed, whereas the concentration of **1a** and **1b** stayed mostly unchanged. After seven hours, full consumption of **2a** was overserved, while more than 50% of **1a** and **1b** remained unreacted, consistent with the absence of **1a** homodimer observed in the model reaction. As the low conversion efficiency in phenol systems was attributed to the fast back electron transfer (BET) in previous reports,[34,35] the rapid charge recombination was believed to be responsible for the lack of reactivity in the phenol component.

The pronounced kinetic difference observed indicates a selectivity, that the alkenyl phenol (**2a**) was activated and underwent subsequent transformation with neutral phenol partners. Relative radical stability was used to rationalise the selectivity (Fig. 5b). The alkenyl phenoxyl radical **6** was found to be thermodynamically more stable by 3.8 kcal mol^{-1} than the comparative phenoxyl radical **15**, most likely due to the extended conjugation enabled by the alkenyl chain. Combined, the kinetic evidence and DFT calculations confirmed that the TiO_2–alkenyl phenol adduct was being photoactivated in the reaction, generating the reactive radical species.

Further investigation on spin density distribution was performed on the alkenyl phenoxyl radical **6** (Fig. 5c). Both NBO and Mulliken spin population indicated that the radical

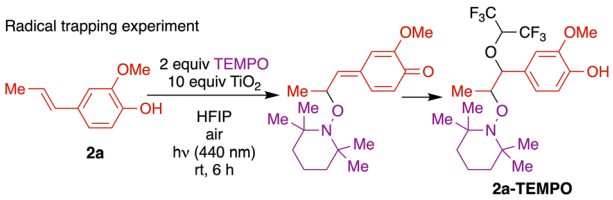

Fig. 6 Mechanistic investigations: radical trapping experiment with TEMPO.

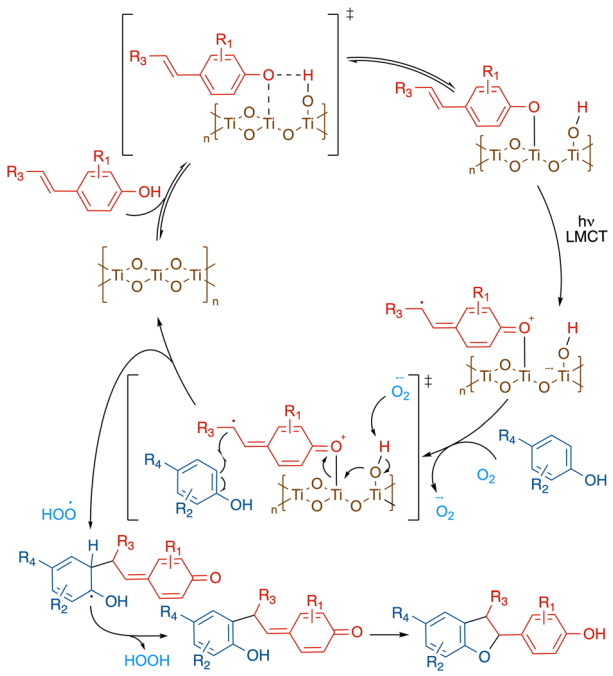

Scheme 4 Proposed catalytic cycle.

character is more concentrated on the β-carbon compared to the *ortho*-site, resulting in a regioselective coupling at the β-site.

To confirm the predicted regioselectivity, a radical trapping experiment was conducted (Fig. 6). Notably, the reaction was markedly inhibited by the addition of radical scavenger 2,2,6,6-tetramethyl-1-piperidinyloxy (TEMPO). Upon surface binding and photoactivation, the resulting alkenyl phenoxyl radical delocalized to the β position was captured by TEMPO. The isolated adduct arising from nucleophilic addition of the solvent to the quinone methide intermediate was characterized, in support of a regioselective radical process. Further, the presence of peroxide formation was confirmed by a positive KI test (see ESI† for details).

To rationalize the absence of a β–β adduct from a potential radical–radical mechanism, the bond dissociation enthalpy (BDE) of the resulting di-*para*-quinone methide was calculated using DFT [UB3LYP-D3/6-31G(d,p), see ESI† for details]. The exceptionally weak β–β C–C bond (9.6 kcal mol^{-1}) indicates the highly unstable nature of the β–β adduct, which could easily undergo rapid homolysis back to the corresponding phenoxyl radical **6**.[36]

On the basis of the above mechanistic studies, a plausible catalytic cycle for this transformation was proposed in Scheme 4. First, the alkenyl phenol binds to the TiO_2 solid surface through the hydroxy group, forming a Ti–O–C linkage.[37] The resulting complex can then be directly activated under visible light *via* ligand-to-metal charge transfer (LMCT), where

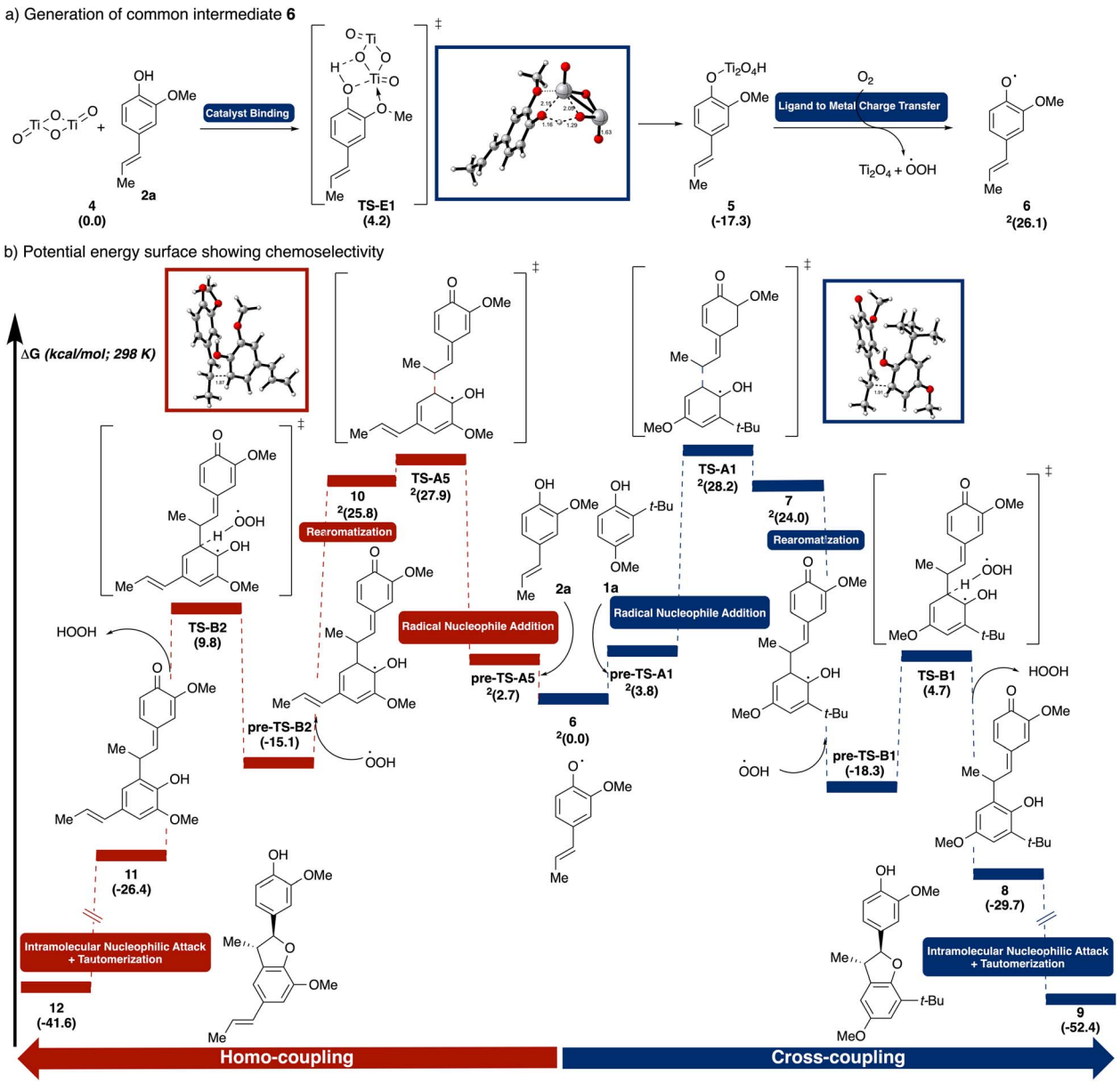

Fig. 7 (a) Formation of common intermediate **6**, (b) formation of cross-coupling and homo-coupling products from **6**. Free energies were computed using UM06/6-311++G(d,p)-SDD(Ti)-CPCM(HFIP)//UB3LYP-D3/6-31G(d,p)-SDD(Ti).

an electron is promoted from the alkenyl phenol HOMO to the TiO_2 conduction band. The terminal oxidant, dioxygen, subsequently collects the extra electron from the TiO_2 conduction band, producing superoxide. The regeneration of the photocatalyst is achieved *via* deprotonation of the titanium-hydroxo adduct by superoxide. The resulting alkenyl phenoxyl radical can then be captured by a neutral phenol nucleophile, forming the pivotal C–C bond. Subsequent hydrogen abstraction by the peroxyl radical rearomatizes the phenol scaffold. And finally, intramolecular nucleophilic attack to the quinone methide constructs the benzofuran ring, which, upon tautomerization affords the final cross-coupling product.

We deployed density functional theory (DFT) calculations [UM06/6-311++G(d,p)-SDD(Ti)-CPCM(HFIP)//UB3LYP-D3/6-31G(d,p)-SDD(Ti), see ESI† for details] to pinpoint key mechanistic steps and to unravel factors governing chemoselectivity. Specifically, the reaction between iso-eugenol (**2a**) and 2-*tert*-butyl-4-methoxyphenol (**1a**) were modeled to represent the general reaction scheme. Conformational searches were performed manually on each structure to locate the lowest energy profiles and only the lowest energy pathways are shown. First, we explored the selectivity in catalyst binding (Fig. 7a). The surface interaction occurs *via* a slightly-uphill transition state **TS-E1** (4.2 kcal mol^{-1}), where the bridging oxygen in TiO_2 deprotonates substrate **2a** while simultaneously forming a Ti–O bond in intermediate **5**. Aided by the coordination of the adjacent methoxy group to the oxophilic Ti, the process was rendered overall downhill in energy (−17.3 kcal mol^{-1}). Comparatively, binding of substrate **1a** to TiO_2 *via* **TS-E2** was found to be overwhelmingly disfavored, both kinetically (9.9 kcal mol^{-1} *vs.* 2.7 kcal mol^{-1}) and thermodynamically (−12.2 kcal mol^{-1} *vs.* −17.3 kcal mol^{-1}), most likely due to the steric hindrance around the *t*-Bu group (see ESI† for details). Photoinduced LMCT of **5** generates the common intermediate alkenyl phenoxyl radical **6**, which is uphill energetically (26.1 kcal mol^{-1}) consistent with the lack of reactivity observed in the absence of light (Table 2, entry 1).

Table 3 TiO_2 recyclability test

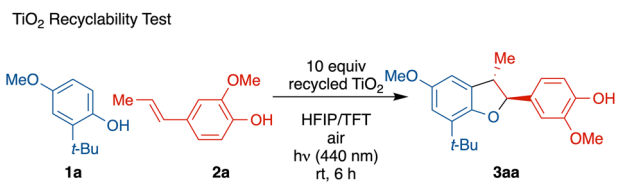

Entry[a]	Yield **3aa**[b] (%)
1	59
2	57
3	63
4	67
5	61

[a] Reaction conditions: **1a** (1.12 mmol), **2a** (0.56 mmol), 4.0 mL solvent. [b] Isolated yield.

Next, from the common intermediate **6**, we investigated the selectivity in coupling (Fig. 7b). Both homo-coupling and cross-coupling pathways were computed as both were observed experimentally. Nucleophilic addition from the *ortho*-position of **1a** to the resonance-stabilized allyl radical **6** proceeds *via* transition state **TS-A1** forming the β-5′ C–C bond. This transition state is stabilized by a CH–π interactions between the *ortho*–*tert*–butyl group of **1a** and the aromatic ring of **6**.

In comparing the cross-coupling and homo-coupling pathways, both the transition states, **TS-A1** (28.2 kcal mol^{-1}) and **TS-A5** (27.9 kcal mol^{-1}), and the resulting intermediates, **7** (24.0 kcal mol^{-1}) and **10** (25.8 kcal mol^{-1}), were found to be close in energy. This finding is consistent with the product mixture observed in the 1 : 1 **1a** : **2a** reaction (Table 1, entry 4). Rearomatization *via* peroxyl radical mediated hydrogen atom abstraction of **7** *via* **TS-B1** forms the more stable **8** (−29.7 kcal mol^{-1}). Subsequent intramolecular attack by the phenol to the quinone methide followed by tautomerization in product **9** drives the energy further downhill (−52.4 kcal mol^{-1}).

To further validate the computational model on product distribution prediction, the key coupling step for another phenol/alkenyl phenol pair was computed. Specifically, the coupling between pterostilbene (**2e**) and 2-*tert*-butyl-4-methoxyphenol (**1a**) was chosen as the reaction afforded only cross-coupling product (see ESI† for details). The absence of homo-coupling can be rationalized *via* both the higher activation barrier (37.8 kcal mol^{-1}) and the higher product free energy (36.6 kcal mol^{-1}) for the homo-coupling.

As radical–nucleophile addition was identified to be the product determining step, we hypothesized that the cross-coupling chemoselectivity would be improved by employing an excess of **1a**. For **1a**, the homo-coupling pathway is far slower due to both less favorable initial coordination to the TiO_2 and faster BET (see above). Indeed, with a 2 : 1 ratio of **1a** : **2a**, cross-coupling yield improved significantly (Table 1, entry 5 *vs.* 4).

Finally, to assess the reusability of the heterogeneous photocatalyst, a TiO_2 recyclability test was conducted through centrifugal separation (Table 3). After five rounds of recycling, no catalyst degradation or loss of reactivity was observed. Upon washing, the recycled TiO_2 showed comparable activity, FT-IR spectrum, and morphology to fresh TiO_2 samples, demonstrating the recyclability and reusability of the photocatalyst (see ESI† for details).

Conclusions

In summary, we developed a novel and single-step method for the synthesis of dihydrobenzofurans with an inexpensive, nontoxic, and recyclable TiO_2 photocatalyst *via* oxidative cross-coupling of phenols with alkenyl phenols. This method leverages the surface interaction between alkenyl phenols and the TiO_2 solid surface which enables direct activation under visible light, obviating the need for pre-functionalization or surface modification. Mechanistic studies including Raman and DRS UV-Vis spectroscopy, kinetics and radical trapping experiments, as well as DFT calculations, support the generation of an alkenyl phenoxyl radical which is captured by a phenol nucleophile.

Notably, the reaction proceeds under benign conditions, with air as the terminal oxidant at room temperature, and is applicable to a broad range of substrates including phenols, anilines, and heterocycles. Moreover, the method is complementary to those in Scheme 2 and functions well with unprotected alkenyl phenols. The resulting 2,3-dihydrobenzofurans are the building blocks of bioactive natural products, and thus are of value in synthetic and pharmaceutical chemistry.

Data availability

The data underlying this study are available in the published article and the ESI.†

Author contributions

JW conceived the topic. JW and YL carried out experiments. YL performed computational studies. All authors reviewed and edited the manuscript.

Conflicts of interest

The authors declare no competing financial interest.

Acknowledgements

We are grateful to the NSF (CHE2102626) and the NIH (R35 GM131902) for financial support of this research and to ACCESS (TG-CHE120052) for computational support. Partial instrumentation support was provided by the NIH and NSF (1S10RR023444, CHE-1827457, 3R01GM118510-03S1, 3R01GM087605-06S1) as well as the Vagelos Institute for Energy Science and Technology and the Singh Center for Nanotechnology. Nicole Bohn (UPenn) is acknowledged for obtaining scanning electron microscope images. Dr Charles W. Ross III (UPenn) is acknowledged for obtaining accurate mass data. Dr Joshua Williams (Drexel University) is acknowledged for obtaining DRS UV-Vis spectra.

Notes and references

1 (*a*) A. Karioti, F. Carta and C. T. Supuran, *Molecules*, 2016, **21**, 1649; (*b*) Z. Huang and J.-P. Lumb, *ACS Catal.*, 2019, **9**, 521; (*c*) W.-T. Wu, L.-M. Zhang and S.-L. You, *Chem. Soc. Rev.*, 2016, **45**, 1570.

2 (*a*) L. B. Davin and N. G. Lewis, *Phytochem. Rev.*, 2003, **2**, 257; (*b*) J.-Y. Pan, S.-L. Chen, M.-H. Yang, J. Wu, J. Sinkkonen and K. Zou, *Nat. Prod. Rep.*, 2009, **26**, 1251; (*c*) R. B. Teponno, S. Kusari and M. Spiteller, *Nat. Prod. Rep.*, 2016, **33**, 1044; (*d*) E. Fuss, *Phytochem. Rev.*, 2003, **2**, 307.

3 (*a*) E. Mnich, N. Bjarnholt, A. Eudes, J. Harholt, C. Holland, B. Jørgensen, F. H. Larsen, M. Liu, R. Manat, A. S. Meyer, J. D. Mikkelsen, M. S. Motawia, J. Muschiol, B. L. Møller, S. R. Møller, A. Perzon, B. L. Petersen, J. L. Ravn and P. Ulvskov, *Nat. Prod. Rep.*, 2020, **37**, 919; (*b*) L. B. Davin, H.-B. Wang, A. L. Crowell, D. L. Bedgar, D. M. Martin, S. Sarkanen and N. G. Lewis, *Science*, 1997, **275**, 362; (*c*) N. G. Lewis and L. B. Davin, *ACS Symp. Ser.*, 1994, **562**, 202.

4 W. C. Neuhaus, A. L. Jemison and M. C. Kozlowski, *ACS Catal.*, 2019, **9**, 11067–11073.

5 (*a*) Q.-B. Liu, X.-X. Huang, M. Bai, X.-B. Chang, X.-J. Yan, T. Zhu, W. Zhao, Y. Peng and S.-J. Song, *J. Agric. Food Chem.*, 2014, **62**, 7796; (*b*) Y.-Y. Lu, Y.-B. Xue, J.-J. Liu, G.-M. Yao, D.-Y. Li, B. Sun, J.-W. Zhang, Y.-F. Liu, C.-X. Qi, M. Xiang, Z.-W. Luo, G. Du and Y.-H. Zhang, *J. Nat. Prod.*, 2015, **78**, 2205; (*c*) L. H. Rakotondraibe, P. R. Graupner, Q.-B. Xiong, M. Olson, J. D. Wiley, P. Krai, P. J. Brodie, M. W. Callmander, E. Rakotobe, F. Ratovoson, V. E. Rasamison, M. B. Cassera, D. R. Hahn, D. G. I. Kingston and S. J. Fotso, *Nat. Prod.*, 2015, **78**, 431; (*d*) L. Zhou, G.-D. Yao, L.-W. Lu, X.-Y. Song, B. Lin, X.-B. Wang, X.-X. Huang and S.-J. Song, *J. Agric. Food Chem.*, 2018, **66**, 11390; (*e*) D. T. Tshitenge, D. Feineis, S. Awale and G. J. Bringmann, *Nat. Prod.*, 2017, **80**, 1604; (*f*) T. Morikawa, I. Hachiman, K. Matsuo, E. Nishida, K. Ninomiya, T. Hayakawa, O. Yoshie, O. Muraoka and T. J. Nakayama, *Nat. Prod.*, 2016, **79**, 2005; (*g*) L. Xiong, C.-G. Zhu, Y.-R. Li, Y. Tian, S. Lin, S.-P. Yuan, J.-F. Hu, Q. Hou, N.-H. Chen, Y.-C. Yang and J.-G. Shi, *J. Nat. Prod.*, 2011, **74**, 1188; (*h*) L. Rao, Y.-X. You, Y. Su, Y. Fan, Y. Liu, Q. He, Y. Chen, J. Meng, L. Hu, Y.-Z. Li, Y.-K. Xu, B. Lin and C.-R. Zhang, *J. Agric. Food Chem.*, 2020, **68**, 8825.

6 (*a*) Y. E. Lee, T. Cao, C. Torruellas and M. C. Kozlowski, *J. Am. Chem. Soc.*, 2014, **136**, 6782; (*b*) H. Shalit, A. Libman and D. J. Pappo, *J. Am. Chem. Soc.*, 2017, **139**, 13404; (*c*) Y. Nieves-Quinones, T. J. Paniak, Y. E. Lee, S. M. Kim, S. Tcyrulnikov and M. C. Kozlowski, *J. Am. Chem. Soc.*, 2019, **141**, 10016; (*d*) J. Wu and M. C. Kozlowski, *ACS Catal.*, 2022, **12**, 6532–6549.

7 F. Saliu, E. L. Tolppa, L. Zoia and M. Orlandi, *Tetrahedron Lett.*, 2011, **52**, 3856–3860.

8 Q. Zhao, J.-K. Jin, J. Wang, F.-L. Zhang and Y.-F. Wang, *Chem. Sci.*, 2020, **11**, 3909–3913.

9 T. R. Blum, Y. Zhu, S. A. Nordeen and T. P. Yoon, *Angew. Chem., Int. Ed.*, 2014, **53**, 11056–11059.

10 P. T. Parvatkar, S. Kandambeth, A. C. Shaikh, I. Nadinov, J. Yin, V. S. Kale, G. Healing, A. H. Emwas, O. Shekhah, H. N. Alshareef, O. F. Mohammed and M. Eddaoudi, *J. Am. Chem. Soc.*, 2023, **145**, 5074–5082.

11 L. Guo, G. Chen, H. Li, C.-H. Tung and Y. Wang, *Green Chem.*, 2023, **25**, 7102.

12 K. Dong, C.-Y. Zhao, X.-J. Wang, L.-Z. Wu and Q. Liu, *Org. Lett.*, 2021, **23**, 2816–2820.

13 (*a*) X. Lang, X. Chen and J. Zhao, *Chem. Soc. Rev.*, 2014, **43**, 473–486; (*b*) D. Friedmann, A. Hakki, H. Kim, W. Choi and D. Bahnemann, *Green Chem.*, 2016, **18**, 5391–5411; (*c*) H. Cheng and W. Xu, *Org. Biomol. Chem.*, 2019, **17**, 9977–9989; (*d*) P. Riente and T. Noel, *Catal. Sci. Technol.*, 2019, **9**, 5186–5232; (*e*) S. Gisbertz and B. Pieber, *ChemPhotoChem*, 2020, **4**, 456–475.

14 (*a*) X. Lang, W. Ma, Y. Zhao, C. Chen, H. Ji and J. Zhao, *Chem.–Eur. J.*, 2011, **18**, 2624–2631; (*b*) X. Lang, W. R. Leow, J. Zhao and X. Chen, *Chem. Sci.*, 2015, **6**,

1075–1082; (*c*) M. Rueping, J. Zoller, D. C. Fabry, K. Poscharny, R. M. Koenigs, T. E. Weirich and J. Mayer, *Chem.–Eur. J.*, 2012, **18**, 3478–3481; (*d*) C. Vila and M. Rueping, *Green Chem.*, 2013, **15**, 2056–2059.

15 (*a*) F. Parrino, A. Ramakrishnan and H. Kisch, *Angew. Chem., Int. Ed.*, 2012, **47**, 7107–7109; (*b*) V. T. Bhat, P. A. Duspara, S. Seo, N. S. B. A. Bakar and M. F. Greaney, *Chem. Commun.*, 2015, **51**, 4383–4385.

16 J. Zoller, D. C. Fabry and M. Rueping, *ACS Catal.*, 2015, **5**, 3900–3904.

17 S. Higashimoto, N. Kitao, N. Yoshida, T. Sakura, M. Azuma, H. Ohue and Y. Sakata, *J. Catal.*, 2009, **266**, 279–285.

18 J. Zhang, H. Chen, M. Liu, T. Lu, B. Gao, X. Yang, L. Zhou, H. Li and Y. Su, *J. Photochem. Photobiol., A*, 2022, **431**, 114005.

19 J. Wu and M. C. Kozlowski, *Org. Lett.*, 2023, **25**, 907–911.

20 M. Ben-Lulu, E. Gaster, A. Libman and D. Pappo, *Angew. Chem., Int. Ed.*, 2020, **59**, 4835–4839.

21 K. Niederer, P. Gilmartin and M. C. Kozlowski, *ACS Catal.*, 2020, **10**, 14615–14623.

22 A. Kirste, B. Elsler, G. Schnakenburg and S. R. Waldvogel, *J. Am. Chem. Soc.*, 2012, **134**, 3571–3576.

23 T. Quell, N. Beiser, K. M. Dyballa, R. Franke and S. R. Waldvogel, *Eur. J. Org Chem.*, 2016, 4307–4310.

24 K. Morimoto, K. Sakamoto, T. Ohshika, T. Dohi and Y. Kita, *Angew. Chem., Int. Ed.*, 2016, **55**, 3652–3656.

25 N. Y. More and M. Jeganmohan, *Org. Lett.*, 2015, **17**, 3042–3045.

26 M. Ziolek, I. Tacchini, M. T. Martınez, X. Yang, L. Sund and A. Douhal, *Phys. Chem. Chem. Phys.*, 2011, **13**, 4032–4044.

27 G. Zhang, G. Kim and W. Choi, *Energy Environ. Sci.*, 2014, **7**, 954–966.

28 S. Kaniyankandy, S. Rawalekar, A. Sen, B. Ganguly and H. N. Ghosh, *J. Phys. Chem. C*, 2012, **116**, 98–103.

29 (*a*) V. C. Vespe and D. F. Boltz, *Anal. Chem.*, 1952, **24**, 664–666; (*b*) N. Hosaka, T. Sekiya, M. Fujisawa, C. Satoko and S. J. Kurita, *J. Electron Spectrosc. Relat. Phenom.*, 1996, **78**, 75–78.

30 B. Z. Chowdhry, J. P. Ryall, T. J. Dines and A. P. Mendham, *J. Phys. Chem. A*, 2015, **119**, 11280–11292.

31 J. Fujisawa, S. Matsumura and M. Hanaya, *Chem. Phys. Lett.*, 2016, **657**, 172–176.

32 Z.-W. Qu and G.-J. Kroes, *J. Phys. Chem. B*, 2006, **110**, 8998–9007.

33 C. Dette, M. A. Pérez-Osorio, C. S. Kley, P. Punke, C. E. Patrick, P. Jacobson, F. Giustino, S. J. Jung and K. Kern, *Nano Lett.*, 2014, **14**, 6533–6538.

34 K. Ohkubo, A. Fujimoto and S. Fukuzumi, *J. Am. Chem. Soc.*, 2013, **135**, 5368–5371.

35 G. Zhang, G. Kim and W. Choi, *Energy Environ. Sci.*, 2014, **7**, 954–966.

36 M. H. Keylor, B. S. Matsuura, M. Griesser, J.-P. R. Chauvin, R. A. Harding, M. S. Kirillova, X. Zhu, O. J. Fischer, D. A. Pratt and C. R. J. Stephenson, *Science*, 2016, **354**, 1260–1265.

37 J. Fujisawa, S. Matsumura and M. Hanaya, *Chem. Phys. Lett.*, 2022, **803**, 139833.